Materials
Views
www.MaterialsViews.com

ADVANCED
FUNCTIONAL
MATERIALS
www.afm-journal.de

FULL PAPER

Universality of Polarization Switching Dynamics in Ferroelectric Capacitors Revealed by 5D Piezoresponse Force Microscopy

Yunseok Kim,* Xiaoli Lu, Stephen Jesse, Dietrich Hesse, Marin Alexe, and Sergei V. Kalinin*

Ferroelectric polarization switching is sensitively affected by phenomena on multiple length scales, giving rise to complex voltage- and time-controlled behaviors. Here, spatially resolved switching dynamics in ferroelectric nanocapacitors are explored as a function of voltage pulse time and magnitude. A remarkable persistence of formal macroscopic scaling laws for polarization switching based on classical models down to nanoscale volumes is observed. These observations illustrate the persistence of the return point memory in the material and allow the thermodynamic parameters of defects controlling switching to be estimated.

1. Introduction

Ferroelectric materials are broadly explored for multiple current and emergent applications including non-volatile ferroelectric memories,[1–3] tunneling elements,[4,5] transducers and actuators.[3,6] Many of the information technology applications are underpinned by the presence of spontaneous polarization which can be hysteretically switched by an external electric field.[2,3,5,7–16] In the electromechanical and energy harvesting applications, reversible and irreversible domain wall dynamics is an important contribution to enhanced electromechanical and dielectric properties.[17–19] Finally, the coupling between polarization and strain, magnetic, and transport properties enables functional ferroelectric device structures.[9,11,16,20]

For all these applications, knowledge of polarization dynamics as controlled by fundamental materials properties and defects is key step towards knowledge-driven materials and device development. On the atomistic level, polarization switching is well-understood through first-principle and molecular dynamic simulations.[21–23] However, practical applications necessitate understanding of fundamental mechanisms of polarization switching in real device structures and role of local (e.g., structural defects) and non-local (e.g., long-range strain interactions) effects.

The complexity of the mesoscopic switching phenomena can be illustrated by a simple example of polarization switching in polycrystalline material. First, nucleation occurs at predetermined locations and grows vertically along the thickness direction.[24] Subsequently, domain grows sideways. These processes are strongly affected by material imperfections, i.e., defects can lower the nucleation barrier. At the same time, defects (in general case, different subset) can hinder domain wall motion resulting in a broad spectrum of collective pinning phenomena.[11,25,26] For materials with multiple ferroelastic variants, the long range-interactions between incompatible domains can result in collective jamming transitions.[27] Finally, in disordered materials, collective reversible and irreversible domain wall dynamics mediated by long-range interactions, frustration, and pinning, are possible.[17] Depending on the nature of the processes involved in polarization switching, the time scales can vary over many orders of magnitude from sub-nanoseconds for domain nucleation to milliseconds for domain wall dynamics and even slower wall creep and aging phenomena.[28,29]

Traditionally, switching dynamics in ferroelectric capacitors is explored by macroscopic current-based electrical measurements. Probing switching polarization as a function of magnitude and length of voltage pulse provides insight into the switching kinetics, as explored by multiple groups.[25,30–32] However, these measurements lack spatially resolved information. Furthermore, miniaturization of the capacitor size below sub-micrometer limit is hindered by detection limits of current amplifiers.[33,34] The alternative approach for probing

Prof. Y. Kim, Dr. S. Jesse, Dr. S. V. Kalinin
The Center for Nanophase Materials Sciences
Oak Ridge National Laboratory
Oak Ridge, Tennessee 37831, USA
E-mail: yunseokkim@skku.edu; sergei2@ornl.gov
Prof. Y. Kim
School of Advanced Materials Science and Engineering
Sungkyunkwan University
Suwon 440-746, Republic of Korea
Prof. X. Lu, Prof. D. Hesse, Dr. M. Alexe
Max Planck Institute of Microstructure Physics
06120 Halle (Saale), Germany
Prof. X. Lu
State Key Discipline Laboratory of Wide Band Gap Semiconductor
Technology, School of Microelectronics
Xidian University, Xi'an 710071, China

polarization dynamics is offered by scanning probe microscopy (SPM) techniques. Recently, several groups explored polarization dynamics in capacitor structures using piezoresponse force microscopy (PFM).[25,35–37] These studies are largely based on the sequential imaging of domain state evolution as a function of bias pulse parameters,[25,35–38] or spectroscopic imaging using switching spectroscopy PFM.[39–43] However, these approaches probe only a very narrow parameter space (e.g., only time or voltage) and have not yet allowed full energy-time scale of polarization switching to be explored.

Here, we develop a comprehensive picture of local switching phenomena in ferroelectric capacitors in a full time-voltage parameter space. Specifically, we develop the multidimensional spectroscopic method that allows to probe switching at each spatial location as a function of both time and bias magnitude, i.e., generate $P(x,y,V,t)$ data sets. This allows to explore actual domain wall motions, including domain wall velocity and directions, within ferroelectric capacitors. In particular, this also allows to explore both local and global switching dynamics at the nanoscale, i.e., local switching dynamics of the local area underneath the SPM probe at a single point, and global switching dynamics (that can in principle be probed through a probe station) over an entire capacitor area of a single capacitor can both be simultaneously analyzed. We call this novel 5D spectroscopic method as a switching dynamics spectroscopy-PFM (SDS-PFM). Using this SDS-PFM, we observe remarkable persistence of macroscopic scaling laws for polarization switching based on Kolmogorov-Avrami type models down to nanoscale volumes in a single capacitor. This universality of switching behavior in a single capacitor manifests as a persistence of dominant microscopic switching pathway in voltage,

time, and space. Finally, we illustrate that the nucleation kinetics and orientation dependence of domain wall velocities can be explored using a level set method (LSM), providing a comprehensive picture of domain dynamics as a function of pulse parameters.

2. Results and Discussion

2.1. Multidimensional PFM for Exploring Switching Dynamics

In order to explore switching dynamics, we have chosen $Pb(Zr_{0.2},Ti_{0.8})O_3$ (PZT) nanocapacitors as shown in **Figure 1**a as a model system. The preparation and overall switching behavior of these structures is discussed elsewhere.[37,44–46] The as-grown domain structures and the switching behavior can be further illustrated in the band-excitation (BE) PFM images and BE piezoresponse spectroscopy (BEPS) spatial maps illustrated in Figure 1.[45] The BE techniques allow rapid acquisition of the full frequency response at each spatial location and, in particular, can also be used as a basis for spectroscopic measurements of local materials responses.[47,48] As shown in Figure 1b,c, as-grown film possesses uniform polarization and piezoresponse amplitude inside and outside capacitors is uniform, indicative of the high quality epitaxial thin film. The typical BE-PFM hysteresis loop is shown in Figure 1d, illustrating well-defined switching behavior manifested in square-shaped hysteresis loops. However, all the information on the voltage and time dependent switching dynamics is hidden in the narrow voltage interval between 1.7 V to 2.0 V. The BEPS spatial maps of both positive
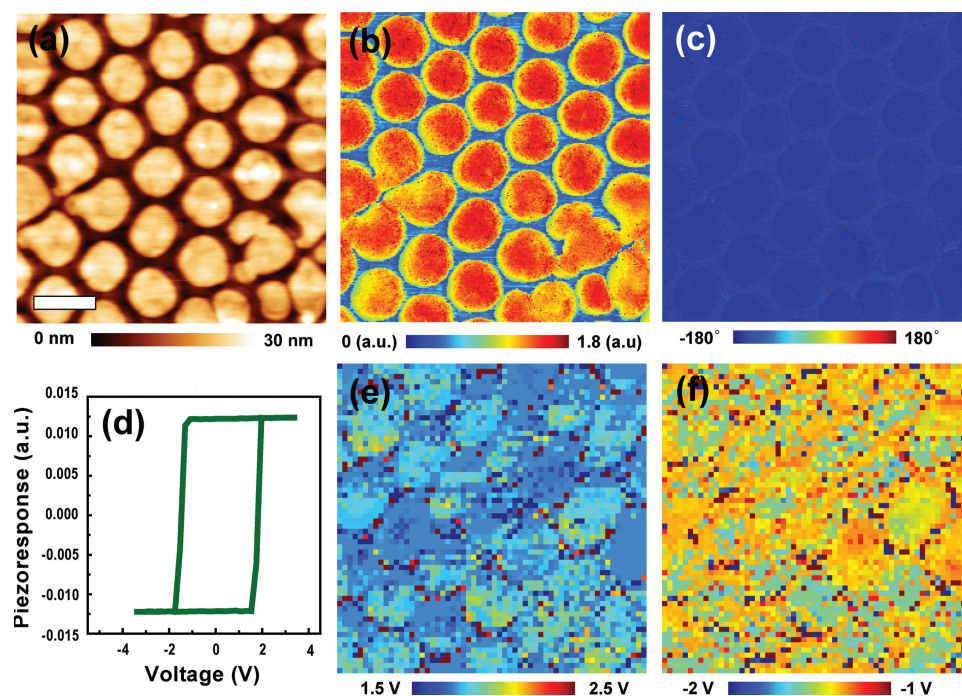

Figure 1. a) Topography, b) BE-PFM amplitude, and c) BE-PFM phase images and BEPS spatial maps of e) positive and f) negative coercive voltages. d) Piezoresponse hysteresis loop of PZT nanocapacitors. Scale bar is 500 nm.
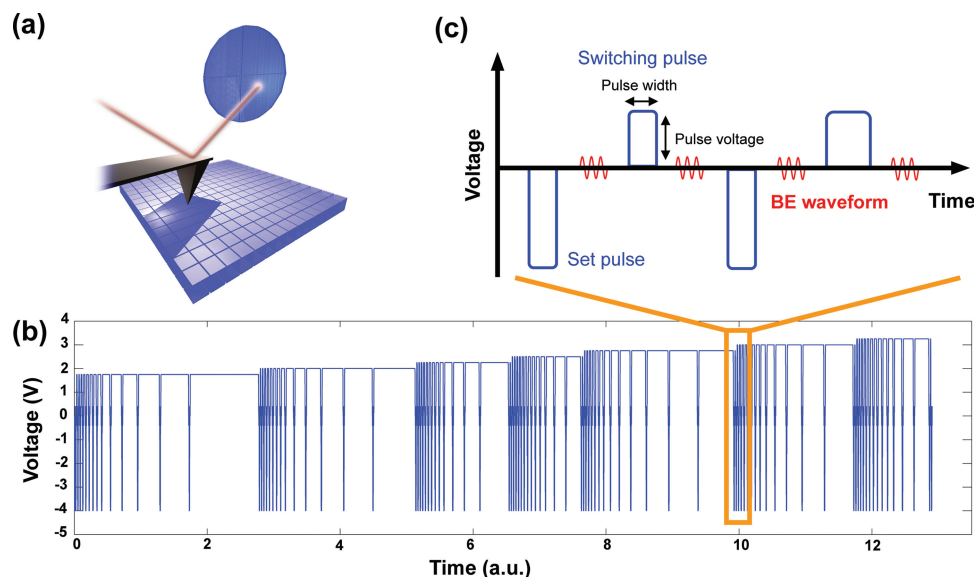
Materials Views
www.MaterialsViews.com

ADVANCED
FUNCTIONAL
MATERIALS
www.afm-journal.de

FULL PAPER

Figure 2. a) Schematic of x–y grid measurement, b) full pulse sequence of each point for SDS-PFM measurements and c) enlarged schematic of waveform. First, the set pulse is applied to form background polarization state. Then, the switching pulse is applied to switch back from the background polarization state. After applying every pulse, the piezoresponse is measured through a BE waveform.

and negative coercive voltages and other parameters quantifying switching behavior also exhibit high uniformity across the film surface (see Figure 1e,f). These observations clearly show that switching events inside capacitors occur within a very narrow voltage window for both signs of applied biases. However, these data do not contain any time-resolved information on the switching process and in particular do not allow a localization of nucleation sites and domain growth dynamics within the capacitor to be established. To explore hidden switching dynamics in the full voltage-time, V–t, domain, we have extended the PFM to probe switching dynamics in the full physical parameter space based on the x-y grid measurement in **Figure 2**a. The switching waveform is shown in Figure 2b. The expanded segment is shown in Figure 2c. The changes in local polarization state are probed using the BE detection after the application of bias pulses. Such a waveform is applied at each spatial location over a 2D spatial grid, giving rise to SDS-PFM. Since switching information (P dependent on the voltage V and time t) is obtained at each spatial location over the x–y grid ($x \times y$) in the BE mode (ω), SDS-PFM yields five dimensional data sets $P(x,y,V,t,\omega)$. This data set can be reduced to 4D data set describing voltage- and time-dependence of polarization dynamics at each location $P(x,y,V,t)$ using standard BE data processing. The BE data processing allows to avoid possible artifacts at the capacitor boundary. which can provide more accurate switching information.

In comparison, in classical PFM approach for studying polarization dynamics, the images are taken after applying each pulse. The imaging typically takes ≈10 min/image, which makes it difficult to observe a metastable status using classical PFM. However, for SDS-PFM implemented here, since the polarization state is probed directly after applying the bias pulse, the present approach allows us to explore even metastable switching information and to acquire both voltage and

time dependent switching dynamics similar to the macroscopic measurements. Note that, in principle, polarization can also be probed in the bias-on state; however, the considerations of rapid data streaming to the external storage preclude continuous capture of bias-on and bias-off polarization states. Furthermore, grid measurements allow the perfect spatial correlation of data with flexible balance between number of spaces, voltage, and time pixels.

To explore the V,t dependent switching dynamics in the PZT nanocapacitors, the following measurement sequences were developed. A –4 V, 4.4 ms pulse is applied as set pulse for the background poling. Then, pulse amplitudes from +1 V to +2.75 V with the pulse widths varying from 4.4 ms to 1.14 s are applied as a train of switching pulses. After each pulse, BE waveforms[47–49] are applied to check their background and then probe the polarization states induced by switching pulses. This pulse sequence is rather similar to the classical pulse sequence in the macroscopic electrical measurements.[32]

Shown in **Figure 3** is a sequence of SDS-PFM phase images describing the polarization evolution in the PZT nanocapacitor. The SDS-PFM phase image after the application of the –4 V set pulse shows complete switching of polarization to the positive state, Figure 3a. The SDS-PFM phase images for +2 V pulse of different length illustrate that the first nucleation event occurs at the capacitor boundary, whereas the second and the third nucleation events occur at the center of the capacitor. On increasing pulse time, the switched area progressively expands in lateral directions. Note that a single SDS-PFM data set contains a sequence of images similar to that in Figure 3 for multiple voltage levels (see Supporting Information Figure S1).

Experimentally, the nucleation sites were shown to be the same for every measurement, suggesting general universality of microscopic switching behavior as discussed in detail below. These pre-determined nucleation sites can be observed through
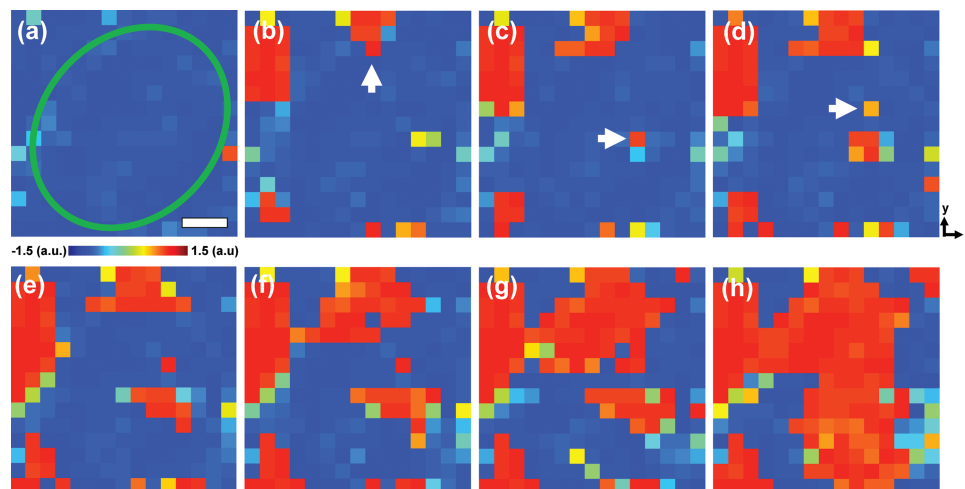
Figure 3. SDS-PFM phase images after applying of a) a set pulse: –4 V with 4.4 ms and b–h) switching pulses: b) 4.4, c) 11, d) 20, e) 60, f) 117, g) 173, and h) 344 ms, respectively, of +2 V. The green line in (a) represents the PZT nanocapacitor. White arrows in (b–d) show nucleation sites. Scale bar is 100 nm.

all of SDS-PFM phase images.[26] At the end stage of domain growth, separately nucleated domains, which are from first, second, and third nucleation sites, are merged (see Figure 3h). Interestingly, domain wall velocity seems to be dependent on the wall orientation (facet of domain), e.g., the domain wall from the second nucleation does not further grow along the +y axis. This effect can be due to the intrinsic crystallographic dependence of wall growth,[50,51] or mediated by local crystal lattice imperfection.[24] For instance, the moving domain walls are caught by dislocations (stop effect),[24] and their interactions depend on the applied field.

2.2. Universality of Global Switching Dynamics

The SDS-PFM data contain the information on the polarization dynamics in the 2D V,t parameter space. Notably, the information can be derived from these data in terms of average and spatially-resolved descriptors. In particular, the multiple studies of polarization switching actively explore the universality of switching behavior for properly chosen renormalization of time by voltage-dependent function.[25,30,32,52,53] Here, we explore whether a similar universality holds globally (i.e., averaged over the capacitor) and locally (i.e., at each location) for switching in capacitors. To obtain the global switching information over the entire capacitor, the total switched polarization change is calculated from the SDS-PFM piezoresponse images. This average switching dynamics is then analogous to the conventional polarization switching obtained by electrical measurements.[25,32] Here, the switching data were analyzed by a Kolmogorov-Avrami-Ishibashi (KAI) (**Figure 4**a) model[25,31,32] and the veracity of the fit was compared to another switching model, i.e., nucleation limited switching (see Supporting Information Figure S2).[32]

The KAI model is the classical switching model which describes the switching behavior as a phase transformation in a finite system and can be described as:

$$P(t) = 1 - \exp\left[-\left(\frac{t}{t_0}\right)^n\right] \quad (1)$$

where $P(t), t_0$, and n are the volume fraction of the switched polarization at time t, characteristic switching time, and the geometric dimension of the domain growth, respectively. The direct application of the KAI model to the SDS PFM data yielded the geometric dimension n in Figure 4b being much lower than 1. This behavior is not unexpected, since KAI dynamics is expected to be applicable to macroscopic systems, whereas in the present case it should be considered as a nominal stretched-exponential (SE) type law.[54,55]

Despite this limitation, the fitted curves in Figure 4a can be used to define the characteristic switching times for each bias level. These correspond to a switching fraction of 1/2. For each $P(t)$ curve, the time axis can be further normalized by the determined characteristic switching time. We note that the characteristic aspect of macroscopic polarization switching is universality, namely the fact that the growth kinetics dP =$f(V,t)$ can be represented as a universal function of a single scaled time dP =$g(t')$, where the normalized time depends on the pulse magnitude. Hence, a small pulse amplitude with a long pulse width gives similar switching as a large pulse amplitude with a short pulse width (see Supporting Information Figure S1). Here, the data sets of Figure 4a are rescaled by a $n \log(t/t_0)$ factor obtained from the SE type law of Equation 1. As shown in Figure 4c, the rescaled data sets fall on a universal curve even for the nanocapacitors,[25] suggesting that the domain growth follows the same behavior as in macroscopic structures despite the fact that only three nucleation centers are active.[25,30,52,53]

We further have explored the activation electric field using an empirical equation based on the SE parameters. It is well known that in macroscopic systems the switching time depends on the electric field as

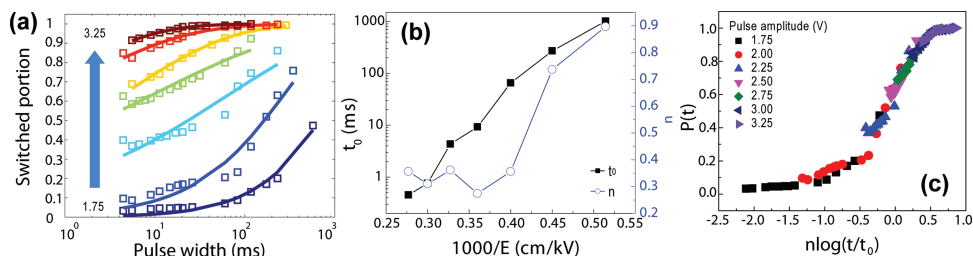$$\tau(E) = \tau_0 \exp\left[\left(\frac{E_a}{E}\right)^\alpha\right] \quad (2)$$

Materials
Views
www.MaterialsViews.com

ADVANCED
FUNCTIONAL
MATERIALS
www.afm-journal.de

Figure 4. a) Time-dependent switched polarization under different amplitude. The dots are obtained from sum of piezoresponse over an entire capacitor and the solid lines correspond to fitted results using SE model. b) SE switching parameters of n and characteristic switching time t_0. c) Rescaled switched polarization using SE fitting parameters.

where τ_0 is a characteristic switching time constant, E_a is the activation electric field, and α is an exponent.[29,32,56,57] Here, we have found that this behavior is observed both locally and globally. This local behavior of the nanocapacitor is clearly visible in **Figure 5**a and the areas near the nucleation sites show low switching time coefficient and activation electric field. We further note that these parameters are phenomenological and likely correspond to biases required to move a domain wall in the disorder potential. The results show that the empirical relationship of Equation 2 can be explored by the present SDS-PFM technique.

2.3. Universality on the Configurations of Domain Growth

The universal curve in Figure 4c represents only the macroscopic state of the system, i.e., the average polarization. Each of these states can correspond to multiple possible domain configurations. However, the universal curve does not show whether each domain configuration is really correlated to each other and how the spatial localization of nucleation and growth processes compare between different field histories. The correlations of each domain configuration can provide further information on the local switching behavior. For instance, if there are strong correlations between intermediate states, we can predict nucleation and subsequent domain wall motion at any given pulse conditions. For each bias-field history, the system starts in the completely un-switched state and ends in the completely switched state. The domain structures in these limiting states are identical. However, the intermediate states can correspond

to different domain configurations, $P_{ij} = P(x,\gamma)$, even for identical average polarization $P = <P(x,\gamma)>$.

To get insight into microscopic mechanisms, *i.e.* the similarity of domain configurations corresponding to each degree of transformation (return point memory),[58] we explore the correlation for the present data set defined as.

$$corr_{x,\gamma} = \frac{E[(P_{mean} - \mu_1) \times (P_{x,\gamma} - \mu_2)]}{P_{x,std} \times P_{\gamma,std}} \quad (3)$$

where $P_{x,\gamma}$, P_{mean}, $P_{x,std}$, $P_{\gamma,std}$, μ_1, and μ_2 are $P(x,\gamma)$, mean of $P(x,\gamma)$, standard deviation of $P(x)$, standard deviation of $P(\gamma)$, EP_{mean}, and $EP_{x,\gamma}$, respectively. $E[X]$ is the mathematical expectation which is the probability-weighted average of the values taken on by X and it can be defined as $E[X] = \sum_{i=1}^{n} t_i\, p_i$ for a random variable X with values $t_1, t_2, \cdots, t_n$ and corresponding probabilities p_i.

If the correlation parameter is 1 for a fixed degree of transformation, this means that the domain configurations are identical, whereas 0 means that the domain configurations are unrelated. The dependence of the switched fraction on pulse parameters is shown in **Figure 6**a, illustrating a gradual increase of switching fraction from zero for low voltages/small times to unity for large voltages/long times. At the same time, the corresponding correlation map of Figure 6b is nearly unity everywhere in the V,t parameter space nearly independent of the degree of switching. This indicates that the microscopic domain configurations follow the same universal dependence, i.e., the microscopic state corresponding to the same degree of transformation does not depend on which combination of pulse magnitude and time was used to establish it. Hence, we conclude that in this case nucleation starts from predetermined sites and domain growth always follows the same patterns.

2.4. Local Switching Dynamics

Once the universality of macroscopic and microscopic switching behavior is established, we further explore the functional form of switching at each point by performing a phenomenological fit of the polarization at each spatial location $P_{ij}(V,t)$ by Equation 1. Shown in **Figure 7**a are spatial maps of the
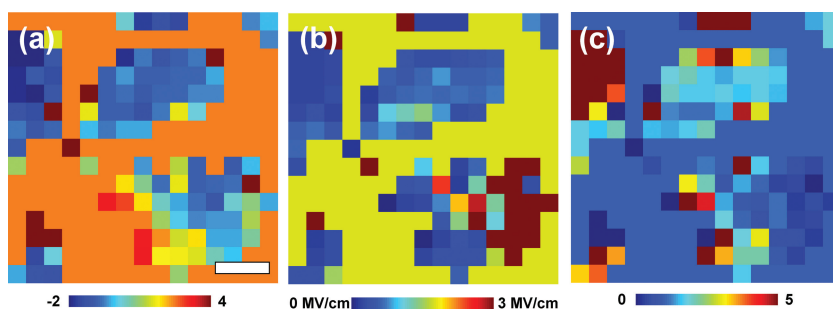

Figure 5. Spatial maps of a) characteristic switching time coefficient $\log(\tau_0)$, b) activation electric field E_a, and c) exponent α. Scale bar is 100 nm.

ADVANCED
FUNCTIONAL
MATERIALS
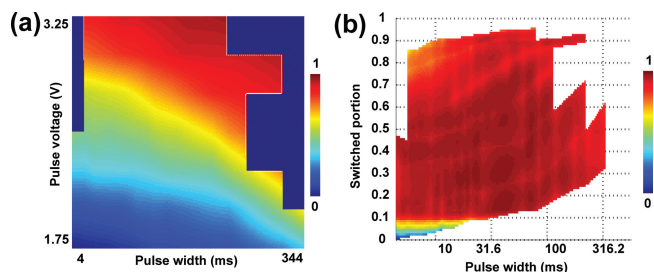www.afm-journal.de

Materials
Views
www.MaterialsViews.com

Figure 6. a) Switched fraction as a function of pulse voltage and width. b) Correlation as a function of pulse width over the entire measured area.

characteristic switching time t_0 obtained by the SE model for each pulse amplitude. The shortest switching time at each pulse amplitude can be found at the same capacitor boundary. In the characteristic switching time maps at +2.00 and +2.25 of Figure 7a,ii,iii, a somewhat darker region can be found at the center of the capacitor which corresponds to the second

and third nucleation sites. The first nucleation event thus occurs at the capacitor boundary while the second and the third ones occur inside the capacitor. Subsequently, three nucleated domains gradually grow laterally. This is identical to the results in Figure 3. In addition to the piezoresponse change, we further directly analyzed the phase change which can show when exactly the phase change occurs. As shown in Figure 7b, the switching behavior is rather similar to that of Figure 7a, which means that the present SE approach reasonably well describes the switching behavior.

From these observations, we can estimate the energetic parameters of defects controlling switching. Under a low pulse voltage, domain wall motion is significantly influenced by the existence of defects. For example, under +1.75 V, a red colored un-switched region passes through the middle of the nanocapacitor as shown in Figure 7a,i, and nucleation sites were separately observed in upper and lower parts, respectively. Then, domains grows into the rest of half nanocapacitor from the nucleation sites. However, under a high pulse voltage, domain
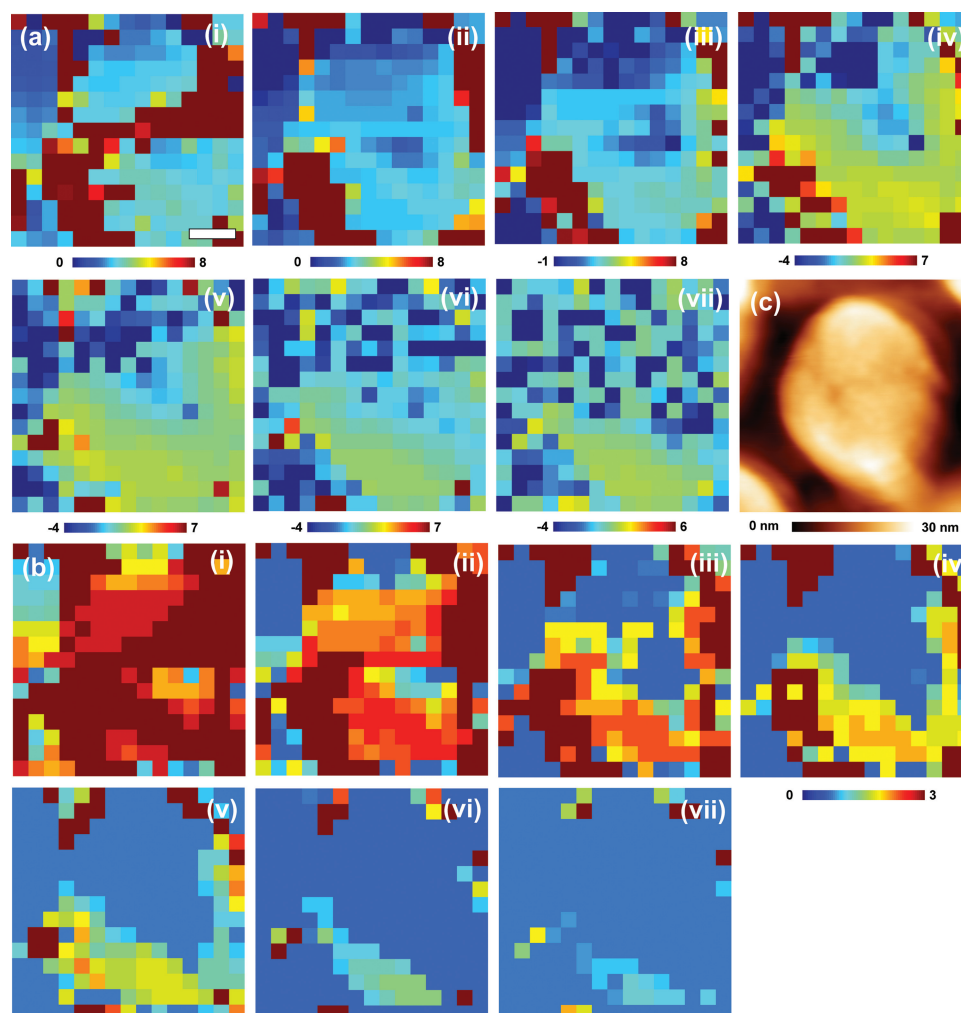

Figure 7. Spatial maps of a) characteristic switching time t_0 and b) nucleation time: i) +1.75 V, ii) +2.00 V, iii) +2.25 V, iv) +2.50 V, v) +2.75 V, vi) +3.00 V, and vii) +3.25 V. The characteristic switching time is obtained from SE switching parameters and the nucleation time is extracted from phase change. c) Corresponding topography image. Scale bar is 100 nm.
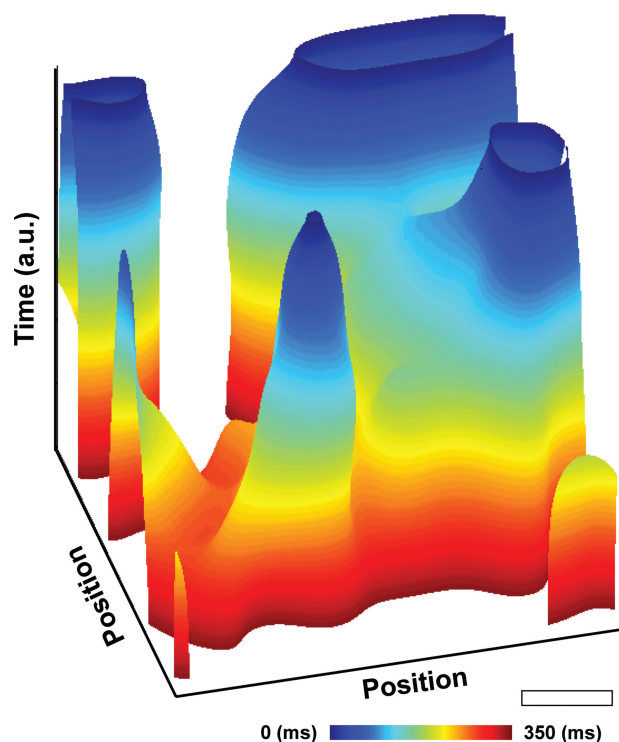
Materials
Views
www.MaterialsViews.com

ADVANCED
FUNCTIONAL
MATERIALS
www.afm-journal.de

Figure 8. Position of domain wall motion for PZT nanocapacitors under +2 V in Figure 3. The domain wall motion was analyzed from SDS-PFM phase images by LSM. Scale bar is 100 nm.

Figure 9. a) Velocity and b) orientation of domain wall motion for PZT nanocapacitors under +2 V in Figure. 3. The white regions and green solid lines represent nucleation sites or non-switched regions and capacitors, respectively. Scale bar is 100 nm.

wall motion. **Figure 9**a,b show more detailed information on the domain wall motion. The white regions represent nucleation or non-switched regions under application of the pulse sequence. The velocity and orientation of domain wall motion from the nucleation sites are very different inside the nanocapacitors. In particular, domain wall orientations are very different even inside capacitors which can be relevant to the "stop effect" observed in macroscopic systems.[32] As shown in the black arrow in Figure 9b, the domain wall cannot cross a certain region. That is why the velocity in this region is relatively much slower than in the surrounding regions as shown in Figure 9a.

3. Conclusion

In summary, we have explored spatially resolved voltage and time dependent switching dynamics in PZT nanocapacitors using 5D PFM, so called SDS-PFM. The obtained results are analogous to macroscopic electrical switching results. The nucleation and subsequent domain wall motions were spatially visualized and analyzed. A universality of ferroelectric switching was observed to hold both on the spatially averaged level and also locally, suggesting the universality of polarization switching pathway independent on details of time-voltage history.

Overall, the SDS PFM approach presented here offers a powerful tool for probing polarization switching in complex systems at high resolutions and can be further adapted for tip-electrode and liquid-electrode PFM. Given the ubiquitous presence of electromechanical responses in other functional oxides including batteries, fuel cells, memristors, etc., this approach can be further used to explore nanoscale phenomena in these systems.

4. Experimental Section

Materials: A 90 nm thick (001) oriented epitaxial PZT thin film was prepared by pulsed laser deposition on SRO(001)/STO substrate. First, the SRO layer was grown at $T \approx 655$ °C, $P_{O2} \approx 0.1$ Torr, $f \approx 5$ Hz and $E \approx 0.7$ J cm^{-2} (KrF excimer laser, $\lambda = 248$ nm). Then, the PZT thin film

wall motion is not affected by the existence of defects. For example, under +2.50 V of Figure 7a,iv, there is not any correlated region with the red-colored region shown in Figure 7a,i. These observations clearly show the energetic aspect of defects on the domain wall motion.

2.5. Multidimensional Domain Wall Motion

Finally, the SDS-PFM data can be used to achieve real-space probing of domain growth dynamics. As mentioned before, the switching process is universal in that virtually the same microscopic domain configurations correspond to fixed degrees of transformation. This allows application of LSM for the visualization and analysis of the SDS-PFM data in Figure 3. The LSM is a numerical technique for tracking interfaces and shapes,[59] and, particularly for the ferroelectric switching, can allow tracking domain wall motion under the aspects of velocity and orientation. Hence, domain wall motion was explored using LSM. **Figure 8** shows the position of domain wall motion, which can show how the domains grow. The nucleation sites can be identified as blue colored peaks. Then, nucleation sites gradually grow sideways, and then these domains are eventually merged as identified in red colored roots. Basically, the LSM provides multidimensional information on the nucleation and subsequent domain wall motion inside the capacitor at one figure.

In addition to the position of domain wall motion in Figure 8, LSM also provides velocity and orientation of domain
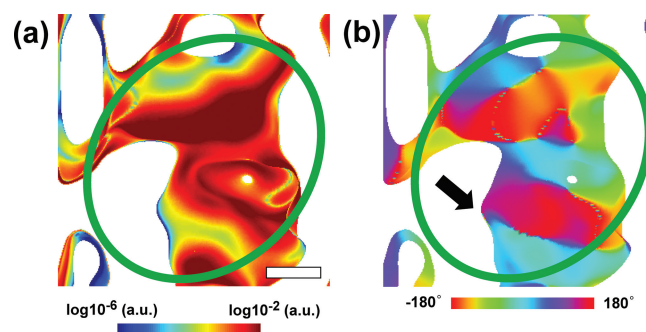
FULL PAPER

was grown at $T \approx 600$ °C, $P_{O2} \approx 0.15$ torr, $f \approx 5$ Hz and $E \approx 1.3$ J cm^{-2}. After deposition of the PZT thin film, the sample was cooled down in a 1 bar O$_2$ atmosphere. 25 nm thick Au/Cu was deposited on top of the thin film through an ultrathin anodic aluminum oxide (AAO) mask by thermal evaporation.[44,46] After removing the AAO mask, film-type Au/Cu/PZT/SRO nanocapacitors with a diameter of around 380 nm were successfully obtained. The detailed fabrication information of the thin films and AAO masks can be found elsewhere.[60]

Measurements: SPM studies were performed with a commercial system (Asylum Research Cypher) additionally equipped with a Labview/Matlab based BE controller.[48] BE-PFM, BEPS, and SDS-PFM were carried out with ≈300 kHz of 0.4V_{pp} BE signal applied to a Pt/Cr-coated probe (Budget sensors Multi75E-G).[43,45] SDS-PFM piezoresponse was obtained from digitized SDS-PFM phase times SDS-PFM amplitude. Then, noisy spikes of SDS-PFM piezoresponse were filtered to reduce the error on the SDS-PFM piezoresponse.

Supporting Information

Supporting Information is available from the Wiley Online Library or from the author.

Acknowledgements

[1] J. F. Scott, C. A. P. Dearaujo, *Science* **1989**, *246*, 1400.

[2] J. F. Scott, *Science* **2007**, *315*, 954.

[3] N. Setter, D. Damjanovic, L. Eng, G. Fox, S. Gevorgian, S. Hong, A. Kingon, H. Kohlstedt, N. Y. Park, G. B. Stephenson, I. Stolitchnov, A. K. Tagantsev, D. V. Taylor, T. Yamada, S. Streiffer, *J. Appl. Phys.* **2006**, *100*, 051606.

[4] E. Y. Tsymbal, H. Kohlstedt, *Science* **2006**, *313*, 181.

[5] V. Garcia, S. Fusil, K. Bouzehouane, S. Enouz-Vedrenne, N. D. Mathur, A. Barthelemy, M. Bibes, *Nature* **2009**, *460*, 81.

[6] D. A. Hall, *J. Mater. Sci.* **2001**, *36*, 4575.

[7] V. Garcia, M. Bibes, L. Bocher, S. Valencia, F. Kronast, A. Crassous, X. Moya, S. Enouz-Vedrenne, A. Gloter, D. Imhoff, C. Deranlot, N. D. Mathur, S. Fusil, K. Bouzehouane, A. Barthelemy, *Science* **2010**, *327*, 1106.

[8] P. Maksymovych, S. Jesse, P. Yu, R. Ramesh, A. P. Baddorf, S. V. Kalinin, *Science* **2009**, *324*, 1421.

[9] C. T. Nelson, P. Gao, J. R. Jokisaari, C. Heikes, C. Adamo, A. Melville, S. H. Baek, C. M. Folkman, B. Winchester, Y. J. Gu, Y. M. Liu, K. Zhang, E. G. Wang, J. Y. Li, L. Q. Chen, C. B. Eom, D. G. Schlom, X. Q. Pan, *Science* **2011**, *334*, 968.

[10] D. Pantel, S. Goetze, D. Hesse, M. Alexe, *Nat. Mater.* **2012**, *11*, 289.

[11] P. Gao, C. T. Nelson, J. R. Jokisaari, S. H. Baek, C. W. Bark, Y. Zhang, E. G. Wang, D. G. Schlom, C. B. Eom, X. Q. Pan, *Nat. Commun.* **2011**, *2*, 1.

[12] S. H. Baek, J. Park, D. M. Kim, V. A. Aksyuk, R. R. Das, S. D. Bu, D. A. Felker, J. Lettieri, V. Vaithyanathan, S. S. N. Bharadwaja, N. Bassiri-Gharb, Y. B. Chen, H. P. Sun, C. M. Folkman, H. W. Jang, D. J. Kreft, S. K. Streiffer, R. Ramesh, X. Q. Pan, D. G. Schlom, M. S. Rzchowski, R. H. Blick, C. B. Eom, *Science* **2011**, *334*, 958.

[13] C. H. Ahn, T. Tybell, L. Antognazza, K. Char, R. H. Hammond, M. R. Beasley, O. Fischer, J. M. Triscone, *Science* **1997**, *276*, 1100.

[14] Y. H. Chu, L. W. Martin, M. B. Holcomb, M. Gajek, S. J. Han, Q. He, N. Balke, C. H. Yang, D. Lee, W. Hu, Q. Zhan, P. L. Yang, A. Fraile-Rodriguez, A. Scholl, S. X. Wang, R. Ramesh, *Nat. Mater.* **2008**, *7*, 478.

[15] C. H. Yang, J. Seidel, S. Y. Kim, P. B. Rossen, P. Yu, M. Gajek, Y. H. Chu, L. W. Martin, M. B. Holcomb, Q. He, P. Maksymovych, N. Balke, S. V. Kalinin, A. P. Baddorf, S. R. Basu, M. L. Scullin, R. Ramesh, *Nat. Mater.* **2009**, *8*, 485.

[16] S. Y. Yang, J. Seidel, S. J. Byrnes, P. Shafer, C. H. Yang, M. D. Rossell, P. Yu, Y. H. Chu, J. F. Scott, J. W. Ager, L. W. Martin, R. Ramesh, *Nat. Nnanotechnol.* **2010**, *5*, 143.

[17] P. Bintachitt, S. Jesse, D. Damjanovic, Y. Han, I. M. Reaney, S. Trolier-McKinstry, S. V. Kalinin, *Proc. Natl. Acad. Sci. USA* **2010**, *107*, 7219.

[18] D. Damjanovic, *Phys. Rev. B* **1997**, *55*, R649.

[19] J. L. Jones, M. Hoffman, J. E. Daniels, A. J. Studer, *Appl. Phys. Lett.* **2006**, *89*, 092901.

[20] H. Lu, C. W. Bark, D. E. de los Ojos, J. Alcala, C. B. Eom, G. Catalan, A. Gruverman, *Science* **2012**, *336*, 59.

[21] M. Sepliarsky, S. R. Phillpot, D. Wolf, M. G. Stachiotti, R. L. Migoni, *Phys. Rev. B* **2001**, *64*, 060101.

[22] B. Meyer, D. Vanderbilt, *Phys. Rev. B* **2001**, *63*, 205426.

[23] M. Sepliarsky, S. R. Phillpot, S. K. Streiffer, M. G. Stachiotti, R. L. Migoni, *Appl. Phys. Lett.* **2001**, *79*, 4417.

[24] A. K. Tagantsev, L. C. Eric, J. Fousek, *Domains in Ferroic Crystals and Thin Films*, Springer, New York **2010**.

[25] J. Jo, H. Han, J. G. Yoon, T. Song, S. H. Kim, T. Noh, *Phys. Rev. Lett.* **2007**, *99*, 257602.

[26] D. J. Kim, J. Y. Jo, T. H. Kim, S. M. Yang, B. Chen, Y. S. Kim, T. W. Noh, *Appl. Phys. Lett.* **2007**, *91*, 132903.

[27] E. K. H. Salje, X. Ding, Z. Zhao, T. Lookman, A. Saxena, *Phys. Rev. B* **2011**, *83*, 104109.

[28] W. J. Merz, *J. Appl. Phys.* **1956**, *27*, 938.

[29] T. Tybell, P. Paruch, T. Giamarchi, J. M. Triscone, *Phys. Rev. Lett.* **2002**, *89*, 097601.

[30] Y. A. Genenko, S. Zhukov, S. V. Yampolskii, J. Schutrumpf, R. Dittmer, W. Jo, H. Kungl, M. J. Hoffmann, H. von Seggern, *Adv. Funct. Mater.* **2012**, *22*, 2058.

[31] Y. Ishibash, Y. Takagi, *J. Phys. Soc. Jpn.* **1971**, *31*, 506.

[32] A. K. Tagantsev, I. Stolichnov, N. Setter, J. S. Cross, M. Tsukada, *Phys. Rev. B* **2002**, *66*, 214109.

[33] S. Tiedke, T. Schmitz, K. Prume, A. Roelofs, T. Schneller, U. Kall, R. Waser, C. S. Ganpule, V. Nagarajan, A. Stanishevsky, R. Ramesh, *Appl. Phys. Lett.* **2001**, *79*, 3678.

[34] H. Kohlstedt, A. Petraru, K. Szot, A. Rudiger, P. Meuffels, H. Haselier, R. Waser, V. Nagarajan, *Appl. Phys. Lett.* **2008**, *92*, 062907.

[35] A. Gruverman, B. J. Rodriguez, C. Dehoff, J. D. Waldrep, A. I. Kingon, R. J. Nemanich, J. S. Cross, *Appl. Phys. Lett.* **2005**, *87*, 082902.

[36] A. Gruverman, D. Wu, J. F. Scott, *Phys. Rev. Lett.* **2008**, *100*, 097601.

[37] Y. Kim, H. Han, W. Lee, S. Baik, D. Hesse, M. Alexe, *Nano Lett.* **2010**, *10*, 1266.

FULL PAPER

[38] I. Stolichnov, L. Malin, E. Colla, A. K. Tagantsev, N. Setter, *Appl. Phys. Lett.* **2005**, *86*, 012902.

[39] S. Jesse, H. N. Lee, S. V. Kalinin, *Rev. Sci. Instrum.* **2006**, *77*, 073702.

[40] K. Seal, P. Bintachitt, S. Jesse, A. Morozovska, A. P. Baddorf, S. Trolier-McKinstry, S. V. Kalinin, *17th IEEE Int. Symp. Appl. Ferroelectrics* **2008**, *1*, 1.

[41] P. Bintachitt, S. Trolier-McKinstry, K. Seal, S. Jesse, S. V. Kalinin, *Appl. Phys. Lett.* **2009**, *94*, 042906.

[42] K. Seal, S. Jesse, M. P. Nikiforov, S. V. Kalinin, I. Fujii, P. Bintachitt, S. Trolier-McKinstry, *Phys. Rev. Lett.* **2009**, *103*, 057601.

[43] S. Jesse, B. J. Rodriguez, S. Choudhury, A. P. Baddorf, I. Vrejoiu, D. Hesse, M. Alexe, E. A. Eliseev, A. N. Morozovska, J. Zhang, L. Q. Chen, S. V. Kalinin, *Nat. Mater.* **2008**, *7*, 209.

[44] Y. Kim, H. Han, B. J. Rodriguez, I. Vrejoiu, W. Lee, S. Baik, D. Hesse, M. Alexe, *J. Appl. Phys.* **2010**, *108*. 042005.

[45] Y. Kim, A. Kumar, O. Ovchinnikov, S. Jesse, H. Han, D. Pantel, I. Vrejoiu, W. Lee, D. Hesse, M. Alexe, S. V. Kalinin, *ACS Nano* **2012**, *6*, 491.

[46] W. Lee, H. Han, A. Lotnyk, M. A. Schubert, S. Senz, M. Alexe, D. Hesse, S. Baik, U. Gosele, *Nat. Nanotechnol.* **2008**, *3*, 402.

[47] S. Jesse, S. V. Kalinin, *J. Phys. D: Appl. Phys.* **2011**, *44*, 464006.

[48] S. Jesse, S. V. Kalinin, R. Proksch, A. P. Baddorf, B. J. Rodriguez, *Nanotechnology* **2007**, *18*, 435503.

[49] S. Jesse, P. Maksymovych, S. V. Kalinin, *Appl. Phys. Lett.* **2008**, *93*, 112903.

[50] S. Kim, V. Gopalan, K. Kitamura, Y. Furukawa, *J. Appl. Phys.* **2001**, *90*, 2949.

[51] K. Kitamura, Y. Furukawa, K. Niwa, V. Gopalan, T. E. Mitchell, *Appl. Phys. Lett.* **1998**, *73*, 3073.

[52] S. Zhukov, Y. A. Genenko, O. Hirsch, J. Glaum, T. Granzow, H. von Seggern, *Phys. Rev. B* **2010**, *82*, 014109.

[53] S. Zhukov, Y. A. Genenko, H. von Seggern, *J. Appl. Phys.* **2010**, *108*, 014106.

[54] A. K. Jonscher, *J. Phys. D-Appl. Phys.* **1999**, *32*, R57;

[55] A. K. Jonscher, *J. Mater. Sci.* **1981**, *16*, 2037.

[56] W. J. Merz, *Phys. Rev.* **1954**, *95*, 690.

[57] H. H. Wieder, *J. Appl. Phys.* **1960**, *31*, 180.

[58] M. S. Pierce, C. R. Buechler, L. B. Sorensen, S. D. Kevan, E. A. Jagla, J. M. Deutsch, T. Mai, O. Narayan, *Phys. Rev. B* **2007**, *75*, 144406.

[59] J. A. Sethian, *Level Set Methods and Fast Marching Methods*, Cambridge University Press, New York **1999**.

[60] X. L. Lu, Y. Kim, S. Goetze, X. G. Li, S. N. Dong, P. Werner, M. Alexe, D. Hesse, *Nano Lett.* **2011**, *11*, 3202.